



## Article

# Estimation of Intertidal Oyster Reef Density Using Spectral and Structural Characteristics Derived from Unoccupied Aircraft Systems and Structure from Motion Photogrammetry

Anna E. Windle <sup>1,\*</sup>, Brandon Puckett <sup>2</sup>, Klaus B. Huebert <sup>1</sup> , Zofia Knorek <sup>3</sup>, David W. Johnston <sup>4</sup> and Justin T. Ridge <sup>4</sup>

<sup>1</sup> Horn Point Laboratory, University of Maryland Center for Environmental Science, Cambridge, MD 21613, USA; khuebert@umces.edu

<sup>2</sup> North Carolina Coastal Reserve and National Estuarine Research Reserve, Beaufort, NC 28516, USA; brandon.puckett@ncdenr.gov

<sup>3</sup> Institute of Marine Sciences, University of North Carolina, Morehead City, NC 28556, USA; zofia@live.unc.edu

<sup>4</sup> Division of Marine Science and Conservation, Duke University Marine Laboratory, Nicholas School of the Environment, Duke University, Beaufort, NC 28516, USA; david.johnston@duke.edu (D.W.J.); justin.ridge@duke.edu (J.T.R.)

\* Correspondence: awindle@umces.edu or awindle110@gmail.com



**Citation:** Windle, A.E.; Puckett, B.; Huebert, K.B.; Knorek, Z.; Johnston, D.W.; Ridge, J.T. Estimation of Intertidal Oyster Reef Density Using Spectral and Structural Characteristics Derived from Unoccupied Aircraft Systems and Structure from Motion Photogrammetry. *Remote Sens.* **2022**, *14*, 2163. <https://doi.org/10.3390/rs14092163>

Academic Editors: Angelica Maria Almeyda Zambrano, Eben Broadbent, Ana Paula Dalla Corte and Carlos Alberto Silva

Received: 21 March 2022

Accepted: 28 April 2022

Published: 30 April 2022

**Publisher's Note:** MDPI stays neutral with regard to jurisdictional claims in published maps and institutional affiliations.



**Copyright:** © 2022 by the authors. Licensee MDPI, Basel, Switzerland. This article is an open access article distributed under the terms and conditions of the Creative Commons Attribution (CC BY) license (<https://creativecommons.org/licenses/by/4.0/>).

**Abstract:** Eastern oysters (*Crassostrea virginica*) are an important component of the ecology and economy in coastal zones. Through the long-term consolidation of densely clustered shells, oyster reefs generate three-dimensional and complex structures that yield a suite of ecosystem services, such as nursery habitat, stabilizing shorelines, regulating nutrients, and increasing biological diversity. The decline of global oyster habitat has been well documented and can be attributed to factors, such as overharvesting, pollution, and disease. Monitoring oyster reefs is necessary to evaluate persistence and track changes in habitat conditions but can be time and labor intensive. In this present study, spectral and structural metrics of intertidal oyster reefs derived from Unoccupied Aircraft Systems (UAS) and Structure from Motion (SfM) outputs are used to estimate intertidal oyster density. This workflow provides a remote, rapid, nondestructive, and potentially standardizable method to assess large-scale intertidal oyster reef density that will significantly improve management strategies to protect this important coastal resource from habitat degradation.

**Keywords:** *Crassostrea virginica*; eastern oyster reefs; oyster density; Unoccupied Aircraft Systems; Structure from Motion photogrammetry; remote sensing

## 1. Introduction

From the mid-Atlantic states in the U.S. through the Gulf of Mexico and the Caribbean, eastern oysters (*Crassostrea virginica*) cluster in fringing reefs located in the intertidal zone [1]. These reefs provide ecosystem services to the surrounding estuarine environment, such as filtering water, stabilizing shorelines, regulating nutrients, and providing habitat for ecologically and economically valuable fish and invertebrates [2–4]. They also support a lucrative fishery, contributing millions of dollars to coastal economies. Once abundant in coastal waters along the U.S. east coast, eastern oysters now face a number of threats from human and environmental stressors. These threats, including overharvesting, predation, disease, pollution, habitat loss or degradation, and climate change, are leading to a decline in oyster populations around the world [5–8]. In the U.S. alone, a 63% decline in the spatial extent of oyster habitat in the past 100 years has been estimated, with the greatest declines happening along Atlantic coast estuarine systems [9]. Effective monitoring of oyster habitat is necessary to ensure the sustainability of this ecologically and economically significant marine species.

Monitoring oyster reef habitats is critical to understanding the complex dynamics of these systems, identifying and tracking changes, and better informing management and restoration efforts. Traditional sampling techniques typically involve intensive field sampling initiatives including mapping reef footprints and height using global navigation satellite systems (GNSS) and calculating oyster density, size structure, and growth rates by manual counts and measurements of individual oyster length within a specified quadrat [10–12]. These methods are labor intensive and can be destructive to the oyster reef environment. Satellite and aerial imagery have been used to map intertidal oyster reef habitat at large scales by manually delineating reef footprints or applying spectral classification methods to distinguish oyster reef habitat from other land cover features [13–17]. However, the coarse resolution of this imagery can potentially exclude small reefs and similar habitat appearance (i.e., oyster reefs appearing similar to adjacent mudflats or salt marshes) can confound classification techniques [15].

Unoccupied aircraft system (UAS) remote sensing is an emerging method to distinguish and map intertidal oyster reefs [18–21]. While not as spatially extensive as satellite or airborne remote sensing, UAS imagery is a low-cost, rapid, and repeatable method to collect data over a large area (e.g., ~25 acres in 20 min with a multirotor UAS, see Windle et al., 2019 [18]). UAS imagery can be collected at a sub-centimeter resolution which results in high overall accuracy in classification techniques [20,21]. UAS imagery has been used to map and quantify intertidal oyster reef extent, however, it also has the potential to provide estimates of oyster density. Spectral characteristics of exposed intertidal oyster reefs can potentially be used to infer reef conditions [13,15–17,22]. Living oyster reefs tend to grow vertically and cast shadows on the surrounding substrate, exhibiting darker hues while unhealthy or dead intertidal oyster reefs are typically composed of more flat, white, reflective shells that have been bleached by the sun [15,17]. Grizzle et al. (2018) [15] related areas of high, medium, and low oyster density to the distinct coloring of intertidal reefs from satellite imagery and found significantly greater live oyster density in reefs exhibiting a dark brown-to-olive signature.

Similarly, the amount of three-dimensional (3D) surface complexity in an intertidal oyster reef can also provide reef condition metrics. Dense reefs containing vertically accreting oysters with increased interstitial spacing typically correlate with healthy reefs allowing for more recruitment, survivorship, and favorable trophic dynamics [23–28]. Colden et al. (2017) [26] demonstrated how structural complexity, or rugosity, impacts biological and physical processes on the reef and found lower rates of sediment deposition on reefs with higher rugosity values.

Spectral and structural metrics of intertidal oyster reefs can be obtained with UAS imagery. Structure from Motion (SfM) is a photogrammetric technique that approximates the 3D structure of an object of interest by identifying key points in individual two-dimensional (2D) images with known camera orientations [29]. UAS-SfM techniques are increasingly being used for coastal research and management, including beach morphology [30], barrier island dynamics and storm impact assessments [31,32], wetland vegetation monitoring [33], and land cover classification [34]. UAS-SfM techniques have recently been used to assist in large-scale intertidal oyster reef habitat classification and mapping [18,20,21], including the application of automated deep learning approaches [35,36]. High resolution point clouds of oyster reefs derived from SfM techniques have also been used to conduct geomorphometric analysis and study how structural complexity influences oyster recruitment and survival [28,37].

The objective of this study was to assess the potential of high resolution spectral and structural characteristics provided by UAS-SfM techniques to estimate intertidal oyster density. To do so, we evaluated the relationship between in situ intertidal oyster density measurements and multiple spectral and structural metrics. Results from this research can assist coastal managers and researchers by providing rapid, remote, and nondestructive intertidal oyster monitoring techniques.

## 2. Materials and Methods

### 2.1. Study Site

Data were collected from natural and restored intertidal oyster patch reefs within the Rachel Carson National Estuarine Research Reserve (NERR) located in Beaufort, NC, USA (Figure 1). The 937 ha Reserve consists of a complex of several small islands on the western and eastern portions of the Reserve, respectively. Town Marsh consists of natural fringing intertidal oyster reefs along the shoreline adjacent to a marsh and maritime forest. Middle Marsh is a relict flood tide delta consisting of a saltmarsh complex with natural fringing reefs and isolated restored patch reefs constructed in 1997 and 2000 [38]. Harvesting oysters is prohibited at Town Marsh but allowed at reefs located in Middle Marsh. We collected data at six natural patch reefs from Town Marsh, ranging in area from 32 to 530 m<sup>2</sup>, and nine natural and restored patch reefs from Middle Marsh, ranging in area from 13 to 303 m<sup>2</sup>.

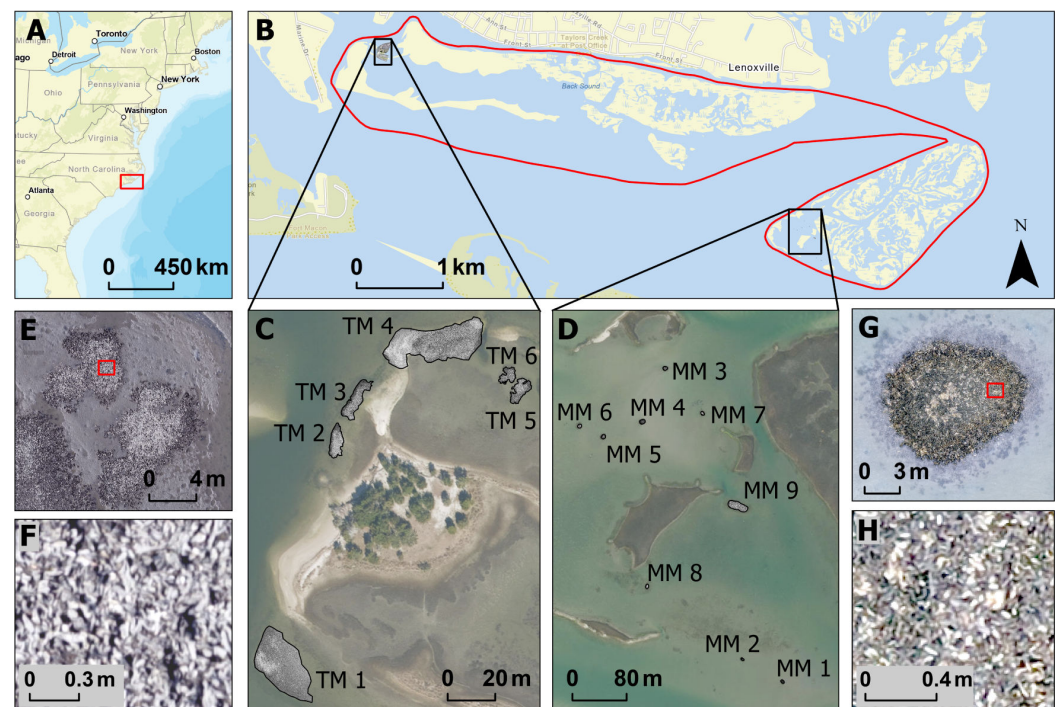


**Figure 1.** (A) Location of study area in eastern North Carolina, USA, (B) Boundary of the Rachel Carson NERR, Beaufort, NC, (C) Natural fringing intertidal oyster reefs located at Town Marsh (labeled and outlined in black), (D) Natural and restored intertidal patch reefs located at Middle Marsh (labeled and outlined in black), (E) UAS imagery showing patch reefs at Town Marsh (TM 5, TM 6, and TM 2), (F) Zoomed in UAS image of TM 6, (G) UAS imagery showing patch reefs at Middle Marsh (MM 3), (H) Zoomed in UAS image of MM 3.

### 2.2. In Situ Data Collection

In situ oyster density data were collected from six natural fringing patch reefs located on Town Marsh in Fall 2017 and Spring 2018 and nine restored or natural reefs located in Middle Marsh in June 2020 (Figure 1). Each reef was sampled by excavating haphazardly placed 0.0625 m<sup>2</sup> (Town Marsh) or 0.04 m<sup>2</sup> (Middle Marsh) quadrats at varying elevations. A range of 1–7 quadrat density measurements was collected at each reef depending on the reef area. A real time kinematic global positioning system (RTK GPS) was used to survey the center of each quadrat location. At both sites, oysters that were located inside the quadrat were sampled to a depth of approximately 15 cm, or to a depth necessary to obtain all live oysters (*sensu* [39]). At Town Marsh, all live oysters were counted and a maximum of 50 live oysters were measured (mm) and at Middle Marsh, all live oysters were counted and measured. The left valve length (LVL), i.e., the distance from the umbo region of

the shell to the anterior shell margin, was measured with calipers to the nearest 0.1 mm. Oyster shell lengths were used to classify oysters into three size classes: recruit (<25 mm), submarket adults (25–76 mm), and market ( $\geq 76$  mm). When multiple excavations took place on a single reef, the counts were averaged. Oyster densities in each size class were calculated by multiplying the proportion of oysters measured in each size class by average total count for that reef. Middle Marsh density measurements were extrapolated to a quadrat size of 0.0625 m<sup>2</sup> to be comparable to Town Marsh measurements.

### 2.3. UAS Remote Sensing and SfM Photogrammetry

UAS flights were conducted over Town Marsh and Middle Marsh during low tidal conditions when most oyster reefs were exposed. UAS flights were conducted over Town Marsh oyster reefs on 29 June 2018, with a DJI S900 hexacopter equipped with a Sony a6000 digital red-green-blue (RGB) camera (ISO ranged from 125–200, shutter speed 1/1250 s) and over Middle Marsh oyster reefs on 1 July 2020 with a DJI Mavic 2 Pro equipped with a Hasselblad L1D-20c RGB camera (ISO 100, shutter speed 1/250–1/500). Flights were automated and imagery was collected with ~75% longitudinal and ~75% latitudinal overlap. The pixel resolution of the Town Marsh and Middle Marsh products were 0.0062 and 0.0073 m, respectively. All UAS operations occurred according to Federal Aviation Administration (FAA) licensing, registration, and renewal processes as dictated by FAA Part 107. At Town Marsh, a total of 15 ground control points (GCPs) were installed and surveyed with an RTK GPS to georectify all UAS surveys and achieve the greatest positional and vertical accuracy. GCPs were made from high-density polyurethane black and white checkerboard tiles (0.0929 m<sup>2</sup>) and situated on PVC pipes of differing lengths evenly distributed around the 2.4 ha survey area (Figure A1). At Middle Marsh, UAS-SfM derived elevations were corrected using a vertical control point measured with an RTK GPS. Horizontal data were referenced to the World Geodetic Datum 1984 (WGS 1984) Universal Transverse Mercator (UTM) Zone 18N, and vertical data were referenced to the North American Vertical Datum established in 1988 (NAVD88). UAS imagery was processed with Pix4D Mapper Pro SfM photogrammetry software v4.2.27 (Prilly, Switzerland) and Drone2Map software v2.3 (ESRI Inc., Redlands, CA, USA) to output georectified RGB orthomosaics and digital elevation models (DEMs). Orthomosaics and DEMs were transferred to ArcGIS Pro 2.4.0 mapping software (ESRI Inc., Redlands, CA, USA) for geospatial analyses. Using the UAS imagery as a reference, individual patch reefs were manually delineated and clipped to form patch reef RGB orthomosaic and DEM raster layers for Town Marsh and Middle Marsh, respectively.

### 2.4. Calculating Spectral and Structural Metrics

Geospatial analyses were performed on the patch reef orthomosaic and DEM layers to calculate spectral and structural metrics. Specific metrics used in this study are described below, however, descriptions and results of all metrics calculated can be found in Appendix A. An unsupervised classification was performed using a modified iterative optimization clustering procedure ('Iso Cluster Unsupervised Classification' tool). This technique organizes the input orthomosaic raster into a user-defined number of clusters to produce signatures which are used to classify the data [40]. The number of classes was set to three to separate pixels representing light, intermediate, and dark colored oysters, the minimum pixels per cluster and sampling interval was set to 20. Variability in the proportions of pixel classifications among sites was expressed as two principal components ('PC1' and 'PC2'), using principal component analysis ('prcomp' function, R v3.5.1). Since the proportions always add up to 100%, there were only 2 degrees of freedom among the three pixel classes. For example, 30% light and 40% dark pixels mean the remaining 30% must be intermediate colored pixels. For this reason, expressing the proportion of pixel classifications as two principal components results in no loss of information. A 'surface complexity' metric was computed using the 'Focal Statistics' tool to calculate neighborhood standard deviation measurements of DEM elevation values using a 161 × 161 (1 m × 1 m)

rectangle pixel window for Town Marsh imagery and a  $137 \times 137$  ( $1 \text{ m} \times 1 \text{ m}$ ) rectangle pixel window for Middle Marsh imagery. A  $1 \text{ m}^2$  area was chosen to investigate the effects of surface complexity since it is a scale of the typical unit for oyster density ( $\# \text{ m}^{-2}$ ). Mean surface complexity was calculated for each reef ( $n = 15$ ) with the ‘Zonal Statistics as Table’ tool using the reef delineation shapefiles as the zone dataset. A higher surface complexity metric is indicative of greater vertical variability and interstitial spacing within  $1 \text{ m}^2$  areas.

### 2.5. Statistical Analysis

A series of generalized additive models (GAMs) (‘mgcv’ package, R v3.5.1) were used to describe the mean in situ density of oysters (response variable) as a linear function of smoothed mean spectral and structural metrics (predictor variables). A GAM is a non-parametric generalization of linear regression that iteratively fits smoothed relationships between dependent and independent variables [41]. In this study, a series of GAMs were constructed using a thin plate spline smoothing with up to 3 degrees of freedom per predictor variable. All predictor variables were tested for collinearity and variables that were strongly correlated were not applied in the same GAM. For GAMs using both PC1 and PC2 as explanatory variables, a combined 2-dimensional smoothing term for a surface with  $\leq 6$  degrees of freedom was used instead of separate 1-dimensional smoothing terms with  $\leq 3$  degrees of freedom per variable. Specifying a gamma distribution for oyster density, a log link function, and maximum likelihood estimation of smoothing parameters resulted in a good fit to the data (based on visual inspection of function ‘gam.check’ diagnostic plots). Due to the log link function, the partial additive effects can be seen as analogous to predicting the log transformed oyster density.

Candidate GAMs were fitted for all possible combinations of predictor variables and for different size classes of oysters. Candidate models with insignificant factors ( $p > 0.05$ ) were excluded and the best models were selected from the remaining candidates based on the highest explained deviance. In cases with multiple factors in the final GAMs, the relative importance of each was estimated by omitting each factor and noting the resulting reduction in explained deviance.

## 3. Results

### 3.1. In Situ Data

Total oyster density across all reefs ranged from 768 to  $6975 \text{ m}^{-2}$ , recruit density ranged from 33 to  $3150 \text{ m}^{-2}$ , submarket density ranged from 481 to  $3475 \text{ m}^{-2}$ , and market density ranged from 75 to  $900 \text{ m}^{-2}$  (Table 1). Average in situ oyster density measurements at Middle Marsh were 2 to 4.5 times higher than density measurements at Town Marsh. Average oyster LVL ranged from 32.4 to 63.1 mm among all reefs.

**Table 1.** Average in situ oyster length, measured as left valve length, density for each size class, spectral and structural metrics calculated for each patch reef located on Town Marsh (TM) and Middle Marsh (MM) that were applied in a series of GAMs.

Patch Reef	Average Length (mm)	Total Density ( $\#/\text{m}^2$ )	Recruit Density ( $\#/\text{m}^2$ )	Sub Market Density ( $\#/\text{m}^2$ )	Market Density ( $\#/\text{m}^2$ )	Light Colored Pixels (%)	Intermediate Colored Pixels (%)	Dark Colored Pixels (%)	Surface Complexity (m)
TM 1	47.9	1184	193	822	169	22	57	22	0.01
TM 2	47.0	971	123	751	97	37	33	30	0.04
TM 3	44.3	2640	792	1373	475	27	32	41	0.04
TM 4	35.4	1944	783	1031	130	42	36	22	0.03
TM 5	56.7	888	161	481	246	24	38	38	0.03
TM 6	63.1	768	33	501	235	27	38	35	0.03

Table 1. Cont.

Patch Reef	Average Length (mm)	Total Density (#/m <sup>2</sup> )	Recruit Density (#/m <sup>2</sup> )	Sub Market Density (#/m <sup>2</sup> )	Market Density (#/m <sup>2</sup> )	Light Colored Pixels (%)	Intermediate Colored Pixels (%)	Dark Colored Pixels (%)	Surface Complexity (m)
MM 1	42.2	5400	2300	2200	900	5	17	78	0.04
MM 2	36.8	5100	2825	1500	775	5	16	79	0.05
MM 3	55.6	1925	675	600	650	12	32	57	0.06
MM 4	52.9	3525	1025	1650	850	6	24	70	0.04
MM 5	57.4	1900	475	700	725	13	37	50	0.05
MM 6	39.4	2475	1025	1125	325	31	43	26	0.04
MM 7	46.6	3100	675	2100	325	31	40	29	0.05
MM 8	32.4	6975	3150	3475	350	41	43	16	0.03
MM 9	40.5	2725	400	2250	75	33	46	21	0.02

### 3.2. Spectral and Structural Metrics

The unsupervised classification of light, intermediate, and dark colored pixels matched visual inspections of UAS oyster reef imagery (Figure A2) with the percentage of light colored pixels ranging from 5 to 42%, percentage of intermediate colored pixels ranging from 16 to 57%, and percentage of dark colored pixels ranging from 16 to 79% (Table 1). The variability of pixel classification expressed as two principal components are shown in Figure A3. The major axis of variability (PC1) explains 92.85% of the total variability in pixel appearance and is driven by the difference between dark pixels to both light and intermediate pixels. The second axis of variability (PC2) is driven by differences in light to intermediate pixels and explains an additional 7.14% of the variability (Figure A3). Mean surface complexity across all reefs ranged from 0.01 to 0.06 m (Table 1).

### 3.3. Comparison to In Situ Density Measurements

For total and recruit oyster size classes, GAMs that incorporated PC1 and surface complexity performed best and explained 73.4% and 72.2% of the deviance in the density of each size class, respectively. In both cases, oyster density was positively associated with surface complexity and negatively associated with intermediate values of PC1 (~38% dark pixels) (Figures 2 and A2). For submarket oysters, a GAM with PC1 as the only explanatory variable performed best and explained 48.5% of the deviance. Submarket oyster density was also lowest at intermediate PC1 values as with the total and recruit size classes. For market oysters, a GAM that incorporated both PC1 and PC2 as well as surface complexity performed best and explained 79.2% of the deviance. Market density was positively associated with surface complexity (as in the other size classes) and positively associated with a high proportion of intermediate (and, to a lesser extent, dark) pixels.

For GAMs with multiple factors, the relative importance of each factor was estimated. For the best performing GAM estimating total oyster density, removing PC1 resulted in a 56.3% reduction in explained deviance, whereas removing surface complexity resulted in a 22.7% reduction in deviance. For the best performing GAM estimating recruit size oyster density, removing PC1 resulted in a 51.2% reduction in deviance, whereas removing surface complexity resulted in a 28.4% reduction in deviance. For the best performing GAM estimating market oyster density, removing PC1 resulted in a 21.7% reduction in deviance, removing PC2 resulted in an 8.6% reduction in deviance, and removing surface complexity resulted in a 16.7% reduction in deviance.

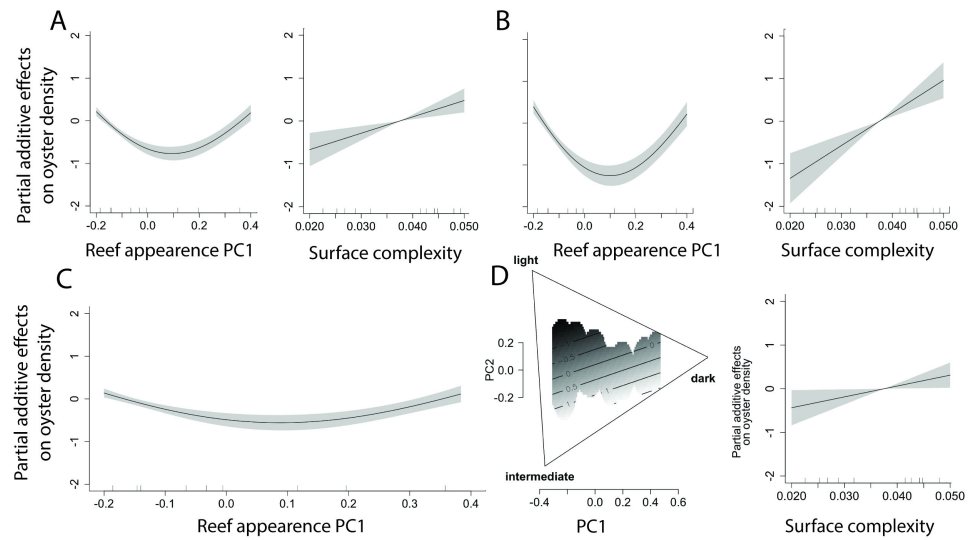


**Figure 2.** Partial additive effects of fitted GAM models by oyster size class: (A) total, (B) recruit (<25 mm), (C) submarket (25–76 mm), (D) market ( $\geq 76$  mm). Tick marks along the x-axis are the observed data points. Gray shading represents  $\pm 2$  standard error confidence bands. Panel (D) includes a PCA plot where contour lines and shading represent partial additive effects on market oyster density, with the darker shading indicating the minimum. Y-axes and contour units are log transformed oyster density due to the log link function applied in the GAM models.

The predicted oyster density derived from the series of GAMs compared well with in situ oyster density for each size class (Figure 3). The GAM used to predict market sized oysters contained the highest correlation when compared to in situ density ( $r^2 = 0.93$ , Figure 3) while the GAM used to predict submarket oyster density had the weakest correlation ( $r^2 = 0.50$ , Figure 3). Although the sample size of reefs was relatively small ( $n = 15$ ), this analysis demonstrates that a combination of spectral and structural metrics derived from UAS-SfM products has the potential to accurately estimate oyster density.

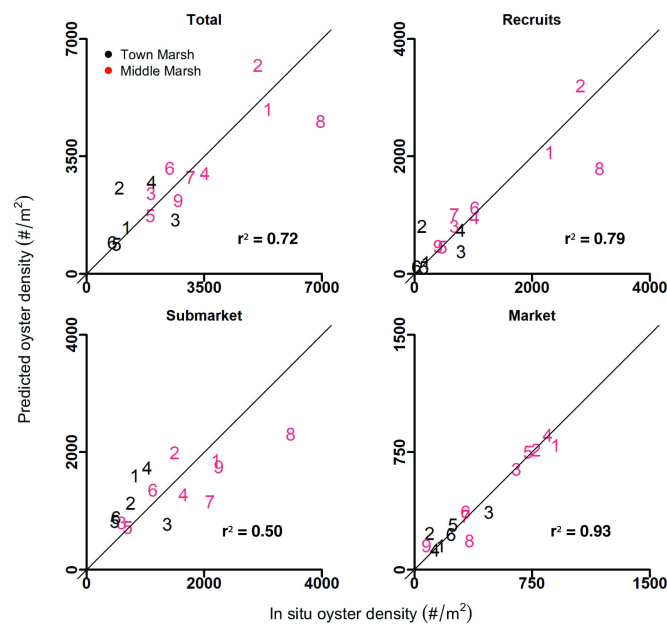


**Figure 3.** Intertidal oyster density predicted from GAMs for each size class total, recruit (<25 mm), submarket (25–76 mm), market ( $\geq 76$  mm) that incorporated spectral and structural metrics derived from UAS and SfM products in relation to in situ oyster density. Black line represents the 1:1 line.

## 4. Discussion

This study details the first remote, rapid, nondestructive, and potentially standardizable framework for estimating intertidal oyster density from UAS-SfM products. Spectral and structural metrics derived from the SfM products were compared against in situ oyster density for different oyster size classes using a series of GAMs. Results have broad implications for large-scale intertidal oyster reef monitoring, but several aspects and caveats of this study merit additional discussion.

### 4.1. Intertidal Oyster Reef Density Estimation

The overall mean live oyster density ( $1383 \# \text{ m}^{-2}$ ) and mean shell height (46.5 mm) across all reefs compare well with recent studies on intertidal oyster reefs in the Rachel Carson Reserve [42] and in other coastal environments [15]. Oyster density measurements differed across reefs and can be tied to differences in reef type (natural vs restored), age of reef, and growth rates. High growth rates on young reefs typically consist of more clustering and higher densities while older and more mature reefs may be operating at their growth ceiling and maintaining elevation with smaller oysters [4,42]. Despite differences in density and size structure among reefs, spectral and structural characteristics generally provided good predictions of size-specific density across reef types and settings.

Past studies have used manual interpretation methods to classify intertidal oyster reefs based on reef appearance in remote sensing imagery [15,17]. Leveraging this relatively subjective technique, the present study relied on machine learning image classification methods to quantify the amount and change of reef appearance or color. A PCA was used to reduce the dimensionality of the unsupervised classification results on the digital count pixel values to lessen the number of variables to apply in a GAM. PC1 is a linear combination of the initial variables of light, intermediate, and dark pixels and when applied in the GAMs used in this study explained 48.5–61.4% of the deviance in oyster density, depending on size class. For total, recruit, and submarket oyster sizes, the partial additive effects on oyster density from PC1 contained a minimum that corresponds to where the proportion of both light and intermediate pixels was similar to dark colored pixels (Figure 2). This minimum describes how oyster density is lowest in areas with an equal mix of light-intermediate and dark pixels, and higher in areas with more light-intermediate colored pixels or more dark colored pixels (Figure A2). If more areas with dead, bleached oyster shells were included in the GAMs (only reef TM4 included sizeable dead shell extent), it is expected that the PCA results would show more variability in light to intermediate pixels and the partial additive effects on oyster density would linearly increase with more dark pixels. For market sized oysters, both principal components were included in the best performing GAM, which contains a minimum that corresponds to where the proportion of light pixels is the greatest. With the maximum corresponding to where the proportion of intermediate and dark pixels is greatest, we see market oyster density increasing with darker reef coloring (Figure 2). This relationship is more apparent in market sized oysters likely due to more clustering and greater shadowing.

Surface complexity explained additional deviance in GAMs for total, recruit, and market oyster densities, demonstrating that structural metrics can generally enhance oyster density estimations. In these GAMs, the partial additive effects of oyster density increased with increasing surface complexity (Figure 2). Surface complexity was considered significant in predicting recruit oyster density, likely because there are more recruits on reefs that have more interstitial spaces that enhance oyster recruitment [43]. Surface complexity was also considered significant in predicting market density likely due to more clustering of larger oysters. Surface complexity was not considered significant in the GAM predicting submarket oyster density, potentially due to a lack of relationship with clustering and more variability in the submarket surface complexity data. The total, recruit, and submarket GAMs predicted MM 8 to have lower oyster density than observed (Figure 3), likely due to MM 8 being a natural reef accumulating more dead shells through time and consisting of a

relatively low proportion of large (market size) oysters to recruits and juveniles resulting in lower surface complexity.

#### 4.2. Limitations and Considerations

There are some important considerations regarding the collection of UAS imagery in coastal environments, such as solar position, shadowing, cloud cover, and tides [44]. Shadowing from nearby vegetation or vertically growing oysters can occur depending on the solar position in the sky. Additionally, the amount of moisture on the oysters can influence glare. To minimize the effect of shadowing and glare, it is recommended to collect UAS imagery close to solar noon and towards or away from the sun azimuth (i.e., the azimuth  $\pm 180^\circ$ ). It is also generally preferable to collect data when illumination conditions are consistent (i.e., clear or completely overcast sky). Variable cloud cover can lead to changes in illumination and potentially influence the spectral characteristics of a reef. Imagery should also be collected at the lowest low tide possible to capture all exposed oyster reefs and limit the effect of surrounding shallow water. It is possible to define shallow submerged reefs in UAS imagery [18], however, the spectral and structural characteristics of those reefs can be significantly influenced by the water column and impact oyster density predictions. Precise manual delineation of oyster reefs can also lessen the influence of water on density estimations. It is possible that oysters located higher in the tidal frame can be exposed and dried longer which may impact spectral characteristics, however, it is likely that they will remain spectrally distinguishable from dead, bleached white reefs.

It is important to note that UAS imagery collected in this study was not radiometrically calibrated. The pixel values used in this study are relative to the conditions in which the data were collected and were subject to changes in light conditions. To compare imagery over time, it becomes important to capture as accurate pixel values as possible and correct for lighting changes. This can be accomplished by obtaining a baseline measurement using a calibration panel with a known reflectance value that can be used to adjust the dataset accordingly [45]. Some UAS sensors also contain an upward facing light sensor that records lighting conditions throughout the flight. This information enables the process of converting digital numbers from raw imagery into normalized surface reflectance measurements which can improve comparisons over time and in different environmental conditions. In this study, the approach of clustering pixels into light, intermediate, and dark was intended to reduce the influence of variability in lighting conditions, however, radiometrically calibrated pixel values may improve results.

It is possible for intertidal oysters to grow differently in various environments. For example, Le Bris et al. (2016) [22] studied the spectral characteristics of wild oyster reefs located on the French Atlantic coast and characterized two types of oyster reefs with different spectral characteristics. The authors studied clusters of dense, vertically growing oysters on mudflats which were dark in color due to being partially covered by mud and horizontally growing oysters in rocky areas which were brighter in color [22]. Both reef structures were considered alive and contained differing spectral signatures. In other studies, including the present study, horizontal white bleached shells are typically considered to be dead reefs [15]. Therefore, oyster density models may need to be regionally specific to retrieve accurate density measurements. It is also essential to validate an oyster density prediction model with regionally specific data. Oyster density is expected to vary across different environments and locations; therefore, one density prediction model can result in erroneous predictions at another site. It is recommended to develop a regional oyster density model by collecting initial measurements of in situ oyster density.

Lastly, the deployment of GCPs can be considered laborious and in some cases, destructive to the coastal environment. Site conditions and management needs may dictate the need for GCPs and the expected accuracy of the resulting products. Windle et al. (2019) [18] demonstrated that reef footprints can be accurately assessed without the use of GCPs, however, the use of GCPs increased the accuracy of reef morphology measurements, particularly

in areas with the presence of water and homogeneous spectral characteristics. The use of GCPs will likely not impact reef appearance; however, it is recommended to use GCPs to obtain an accurate surface complexity metric to improve oyster density estimations. Deploying permanent GCPs in a site could lessen the amount of labor and destruction to the reef.

#### 4.3. Management Implications

Intertidal oyster reefs are a critical habitat and are sensitive to anthropogenic impacts. Studies have shown that recreational boat waves can displace live oyster clusters, leading to reef degradation [13]. If intertidal reefs are allowed to be harvested, methods, such as dredges or hand and patent tonging, which scrape living oysters off the reef, can also damage reef structures [46]. Ridge et al. (2015) [42] demonstrated how increasing rates of sea level rise could eventually outpace reef accretion and ultimately exacerbate intertidal oyster reef habitat loss. Thus, it is imperative to monitor intertidal oyster reef density to better manage and protect this marine resource.

Coastal management and restoration practitioners can use commercial grade UAS to conduct quick, inexpensive, and nondestructive surveys to collect high resolution imagery of intertidal reefs. Two-dimensional imagery can assist in targeting priority areas for further sampling, assessing reef extent, and conducting habitat classification [18,20]. Transforming 2D imagery into high resolution 3D models allows for more comprehensive monitoring by providing valuable reef elevation measurements. In addition to estimating oyster density as shown in this study, high resolution 3D models can also be used to emulate the conventional chain-and-tape method to calculate rugosity. In this context, rugosity has been estimated by placing a fine link chain over a reef, allowing it to conform to the crevices and interstitial spaces, and dividing the length of the chain by the reef's linear length to produce an index of rugosity [26,47]. Rugosity values typically range from 1 (i.e., completely flat surface) and increase with higher surface complexity. SfM products can be used to produce a digital chain-and-tape rugosity metric by calculating the sum of elevation per pixel along a linear transect divided by the transect's linear length (Figure 4). Rugosity values derived from this digital chain-and-tape method were not included in the GAMs since it only covers one axis of the reef, however, managers should consider this novel technique for comparisons with measures derived from conventional chain-and-tape methods.

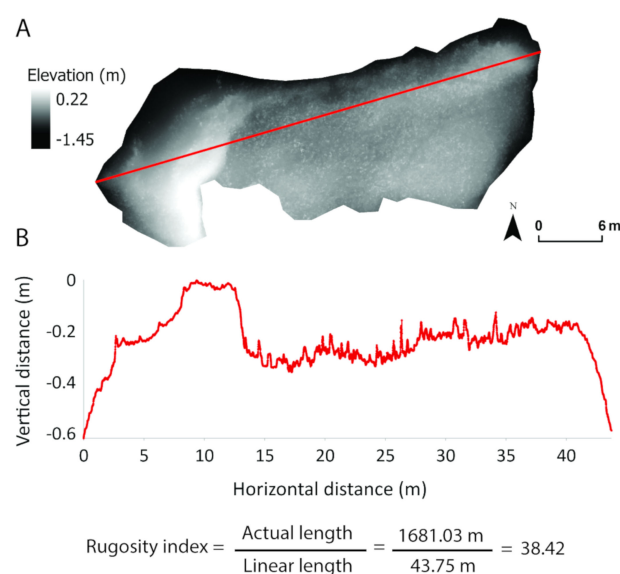


**Figure 4.** Digital chain-and-tape method to calculate an intertidal oyster rugosity index which can be calculated by dividing the actual length (B) from the linear length (A).

UAS and SfM methods can also be combined with UAS light detection and ranging (LiDAR) to enhance oyster density predictions. Aerial LiDAR bathymetry has been shown to differentiate between various geomorphological bedforms [48] and has been used to effectively map intertidal oyster reef habitats [49]. High resolution LiDAR provided by a low-altitude UAS may improve oyster density estimations in shallow subtidal oyster density measurements.

#### 4.4. Future Work

In this study, a digital single-lens reflex camera collected imagery in broad RGB wavebands. Future studies should investigate the utility of using multispectral or hyperspectral imagery. Multispectral sensors can collect imagery in discrete spectral wavebands while hyperspectral sensors collect data in hundreds of narrow wavelengths. Chand et al. (2020) [21] used a multispectral sensor on a UAS and found that intertidal oyster reefs have a strong spectral reflectance in the blue band which was used to distinguish reef habitat from other habitat types. Le Bris et al. (2015) [22] found differences in NIR hyperspectral reflectance between horizontally and vertically growing oysters likely due to less sedimentation on vertically growing oysters. Differences in the magnitude and shape of multispectral or hyperspectral reflectance spectra can potentially enhance estimations of intertidal oyster density. Future studies could also investigate integrating spectral data with synthetic aperture radar (SAR) imagery. SAR is radar backscattering which can provide information on surface parameters, such as roughness. Choe et al. (2012) [50] demonstrated that polarization characteristics of SAR images can effectively distinguish the surface roughness of intertidal oyster reefs from the surrounding mudflat habitat. The integration of high resolution multi or hyperspectral imagery with high resolution elevation or texture data, such as SAR has the potential to improve estimates of large-scale oyster density.

Automated assessment of a coastal ecosystem using machine learning is an emerging field, and Ridge et al. (2020) [35] developed and trained a convolutional neural network to successfully and rapidly classify and measure intertidal oyster reef area from high resolution UAS imagery. Future studies should focus on integrating structural datasets and a well performing oyster density model into a deep neural network to enhance large-scale intertidal oyster density assessment. These methods will be powerful for extensive coastal zone management and monitoring change in habitat over time.

## 5. Conclusions

Through the long-term consolidation of densely clustered shells, oyster reefs provide three-dimensional and complex structures that provide a suite of ecosystem services. Monitoring natural and restored oyster habitats is essential to track changes in habitat and ensure restoration and management goals are being met. In this study, a series of GAMs incorporating spectral and structural metrics of intertidal reefs derived from UAS-SfM outputs demonstrate how intertidal oyster density can be accurately estimated. This workflow provides a remote, rapid, nondestructive, and potentially standardizable method to assess large-scale intertidal oyster reef density that will significantly improve management strategies to protect this important coastal resource from habitat degradation.

**Author Contributions:** Conceptualization, A.E.W., B.P. and J.T.R.; Data curation, A.E.W., B.P., Z.K. and J.T.R.; Formal analysis, A.E.W. and K.B.H.; Funding acquisition, A.E.W., D.W.J. and J.T.R.; Methodology, A.E.W., B.P., K.B.H. and J.T.R.; Project administration, J.T.R.; Resources, D.W.J.; Supervision, D.W.J.; Writing—original draft, A.E.W.; Writing—review & editing, B.P., K.B.H., D.W.J. and J.T.R. All authors have read and agreed to the published version of the manuscript.

**Funding:** This research was funded by North Carolina Sea and Space Grant Graduate Fellowship, (Grant # 2017-R/MG-1710) and the North Carolina Coastal Recreational Fishing License Grants Program (Marine Resources Fund, Grant # 2017-H-068).

**Data Availability Statement:** All imagery and associated data are stored on Duke Digital Repository at <https://doi.org/10.7924/r4223221q>.

**Acknowledgments:** We thank Julian Dale for UAS flight planning and piloting. We also thank Sarah Poulin for assisting in fieldwork and providing valuable contributions through the development of the project. We thank Wendy Folfas, Kelly Dobroski, Claire Atkins-Davis, and Virginia Pan for assisting in fieldwork.

**Conflicts of Interest:** The authors declare no conflict of interest.

## Appendix A

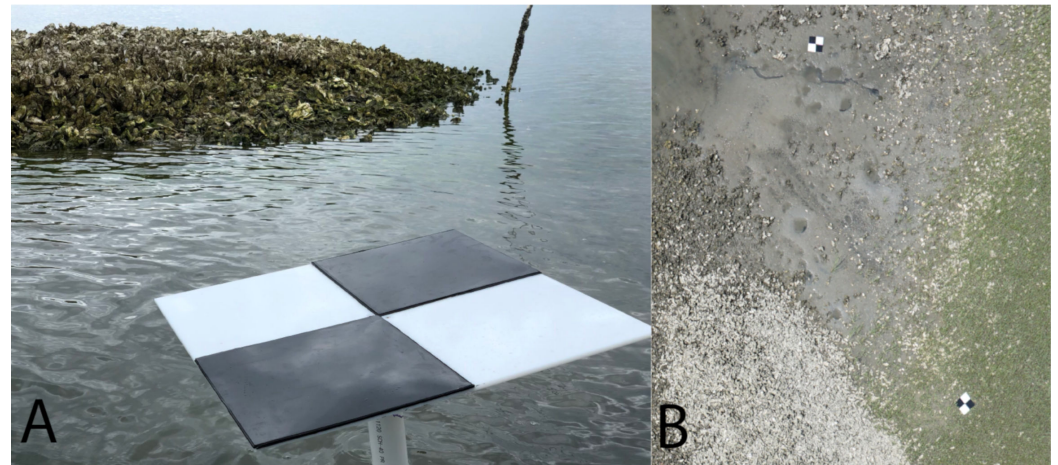


**Figure A1.** (A) GCP deployed in Town Marsh, (B) GCPs from UAS imagery collected in Town Marsh.

Several other spectral and structural metrics were calculated but not included in analyses for the following reasons. The effect of segmentation was studied by applying an unsupervised classification to segmented RGB pixel values of the intertidal oyster reef imagery. Pixels in the patch reef orthomosaic raster layers were segmented using the ‘Segment Mean Shift’ tool with a spectral and spatial detail parameter of 20. Town Marsh imagery was segmented using a minimum segment size of 161 (1 m) and Middle Marsh imagery was segmented using a minimum segment size of 137 (1 m). An unsupervised classification classified the segmented pixels into three separate classes using the same classification parameters listed in the Methods. The classified pixel values derived from the segmented imagery were highly correlated with the raw classified pixel values ( $r > 0.96$ ) and were, therefore, not included in subsequent analyses.

The mean and standard deviation of reef elevation measurements was calculated using the ‘Zonal Statistics as Table’ tool with the DEM reef layer as the zone dataset. While these measurements represent reef wide elevation variability, they are not as representative as the surface complexity metric described in the Methods and were therefore not included in the GAMs. The slope was computed as the maximum rate of change in elevation from a cell to its immediate neighbors using a default  $3 \times 3$  pixel window which translates to  $0.019 \text{ m} \times 0.019 \text{ m}$  at Town Marsh and  $0.022 \text{ m} \times 0.022 \text{ m}$  at Middle Marsh. Rugosity was computed following Burns et al. (2015) as the ratio of 3D surface area to the 2D planar area for each patch reef and was computed by using the ‘Add Surface Information’ tool to all delineated patch reef DEMs. Two patch reefs in Town Marsh (TM2 and TM3) had higher than average slope and rugosity values, likely due to the effect of a small processing window that produced high measurements when averaged over the entire reef. Therefore, slope and rugosity were not included in the GAMs.

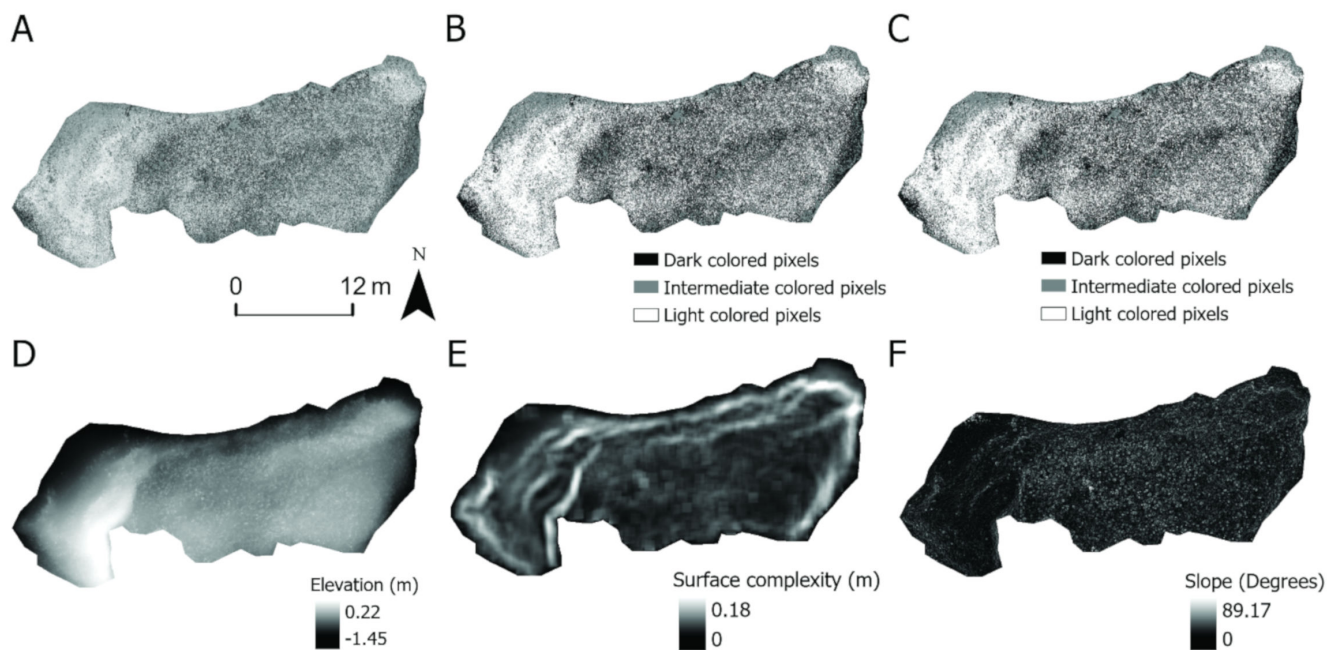


**Figure A2.** Spectral and structural geospatial analyses applied to a patch reef located on Town Marsh (TM 4). (A) RGB orthomosaic with pixel resolution of 0.0062 m. (B) Unsupervised classification on RGB orthomosaic. (C) Unsupervised classification on segmented RGB orthomosaic. (D) Digital elevation model with pixel resolution of 0.0062 m. (E) Surface complexity (neighborhood standard deviation) using a 1 m<sup>2</sup> pixel window. (F) Slope of elevation in a 0.019 × 0.019 (3 × 3 pixel) window.

**Table A1.** Spectral and structural metrics applied in GAMs.

Patch Reef	Average Length (mm)	Total Density (#/m <sup>2</sup> )	Recruit Density (#/m <sup>2</sup> )	Sub Market Density (#/m <sup>2</sup> )	Market Density (#/m <sup>2</sup> )	Light Colored Pixels (%)	Intermediate Colored Pixels (%)	Dark Colored Pixels (%)
TM 1	47.9	1184	193	822	169	22	57	22
TM 2	47.0	971	123	751	97	37	33	30
TM 3	44.3	2640	792	1373	475	27	32	41
TM 4	35.4	1944	783	1031	130	42	36	22
TM 5	56.7	888	161	481	246	24	38	38
TM 6	63.1	768	33	501	235	27	38	35
MM 1	42.2	5400	2300	2200	900	5	17	78
MM 2	36.8	5100	2825	1500	775	5	16	79
MM 3	55.6	1925	675	600	650	12	32	57
MM 4	52.9	3525	1025	1650	850	6	24	70
MM 5	57.4	1900	475	700	725	13	37	50
MM 6	39.4	2475	1025	1125	325	31	43	26
MM 7	46.6	3100	675	2100	325	31	40	29
MM 8	32.4	6975	3150	3475	350	41	43	16
MM 9	40.5	2725	400	2250	75	33	46	21

Table A1. Cont.

Patch reef	Light colored segmented pixels (%)	Intermediate colored segmented pixels (%)	Dark colored segmented pixels (%)	Mean elevation (m)	Standard dev of elevation (m)	Surface complexity (m)	Slope (°)	Rugosity (3D/2D)
TM 1	20	53	27	−0.30	0.06	0.01	8.9	1.03
TM 2	36	30	33	−0.35	0.15	0.04	43.79	4.23
TM 3	25	28	46	−0.34	0.15	0.04	34.6	3.66
TM 4	43	33	24	−0.28	0.17	0.03	13.8	1.09
TM 5	22	32	45	−0.27	0.07	0.03	16.1	1.14
TM 6	25	32	42	−0.23	0.08	0.03	16.0	1.13
MM 1	5	18	78	−0.02	0.09	0.04	12.5	1.04
MM 2	4	17	79	−0.38	0.10	0.05	13.8	1.05
MM 3	11	35	54	−0.20	0.13	0.06	13.1	1.05
MM 4	6	25	69	−0.04	0.12	0.04	11.2	1.04
MM 5	13	40	48	0.20	0.12	0.05	11.3	1.03
MM 6	32	45	23	−0.19	0.11	0.04	9.5	1.02
MM 7	31	39	31	0.09	0.12	0.05	10.9	1.03
MM 8	43	43	14	−0.18	0.08	0.03	7.3	1.01
MM 9	35	47	18	−0.12	0.11	0.02	5.8	1.01

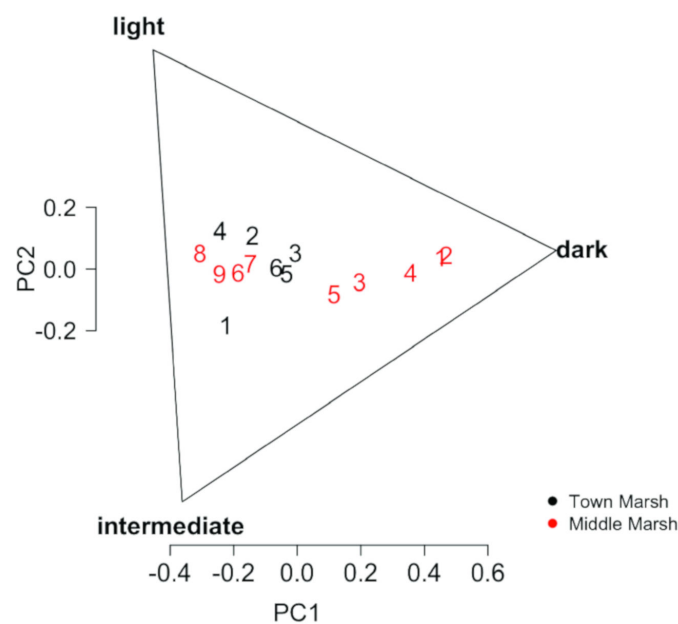


**Figure A3.** PCA on proportions of digital count RGB pixel values classified as light, intermediate, and dark colored pixels for each patch reef.

## References

- Byers, J.E.; Grabowski, J.H.; Piehler, M.F.; Hughes, A.R.; Weiskel, H.W.; Malek, J.C.; Kimbro, D.L. Geographic Variation in Intertidal Oyster Reef Properties and the Influence of Tidal Prism. *Limnol. Oceanogr.* **2015**, *60*, 1051–1063. [[CrossRef](#)]
- Grabowski, J.H.; Peterson, C.H. Restoring Oyster Reefs To Recover Ecosystem Services. *Ecosyst. Eng: Plants Protists* **2007**, *4*, 281–298.
- Grabowski, J.H.; Brumbaugh, R.D.; Conrad, R.F.; Keeler, A.G.; Opaluch, J.J.; Peterson, C.H.; Piehler, M.F.; Powers, S.P.; Smyth, A.R. Economic Valuation of Ecosystem Services Provided by Oyster Reefs. *Bioscience* **2012**, *62*, 900–909. [[CrossRef](#)]
- Ridge, J.T.; Rodriguez, A.B.; Fodrie, F.J. Evidence of Exceptional Oyster-Reef Resilience to Fluctuations in Sea Level. *Ecol. Evol.* **2017**, *7*, 10409–10420. [[CrossRef](#)] [[PubMed](#)]
- Winslow, F. Deterioration of American Oyster-Beds. *Pop. Sci. Mon.* **1881**, *20*, 29–43.

6. Mackenzie, C.L. Causes Underlying The Historical Decline In Eastern Oyster (*Crassostrea Virginica* Gmelin, 1791) Landings. *J. Shellfish Res.* **2007**, *26*, 927–938. [CrossRef]
7. Wilberg, M.J.; Livings, M.E.; Barkman, J.S.; Morris, B.T.; Robinson, J.M. Overfishing, Disease, Habitat Loss, and Potential Extirpation of Oysters in Upper Chesapeake Bay. *Mar. Ecol. Prog. Ser.* **2011**, *436*, 131–144. [CrossRef]
8. Beck, M.W.; Brumbaugh, R.D.; Airoidi, L.; Carranza, A.; Coen, L.D.; Crawford, C.; Defeo, O.; Edgar, G.J.; Hancock, B.; Kay, M.C.; et al. Oyster Reefs at Risk and Recommendations for Conservation, Restoration, and Management. *BioScience* **2011**, *61*, 107–116. [CrossRef]
9. Zu Ermgassen, P.S.E.; Spalding, M.D.; Blake, B.; Coen, L.D.; Dumbauld, B.; Geiger, S.; Grabowski, J.H.; Grizzle, R.; Luckenbach, M.; McGraw, K.; et al. Historical Ecology with Real Numbers: Past and Present Extent and Biomass of an Imperilled Estuarine Habitat. *Proc. R. Soc. B Biol. Sci.* **2012**, *279*, 3393–3400. [CrossRef]
10. Puckett, B.J.; Eggleston, D.B. Marine and Coastal Fisheries Dynamics, Management, and Ecosystem Science Oyster Demographics in a Network of No-Take Reserves: Recruitment, Growth, Survival, and Density Dependence. *Mar. Coast. Fish.* **2012**, *4*, 605–627. [CrossRef]
11. Baggett, L.P.; Powers, S.P.; Brumbaugh, R.; Coen, L.D.; DeAngelis, B.; Green, J.; Hancock, B.; Morlock, S. *Oyster Habitat Restoration Monitoring and Assessment Handbook*; The Nature Conservancy: Arlington, VA, USA, 2007; p. 96.
12. Peters, J.W.; Eggleston, D.B.; Puckett, B.J.; Theuerkauf, S.J. Oyster Demographics in Harvested Reefs vs. No-Take Reserves: Implications for Larval Spillover and Restoration Success. *Front. Mar. Sci.* **2017**, *4*, 326. [CrossRef]
13. Grizzle, R.E.; Adams, J.R.; Walters, L.J. Historical Changes in Intertidal Oyster (*Crassostrea Virginica*) Reefs in a Florida Lagoon Potentially Related to Boating Activities. *J. Shellfish Res.* **2002**, *21*, 749–756.
14. NOAA Coastal Services Center. Pilot Investigation of Remote Sensing for Intertidal Oyster Mapping in Coastal South Carolina: A Methods Comparison. 2003. Available online: <https://coast.noaa.gov/data/digitalcoast/pdf/oyster-mapping.pdf> (accessed on 16 March 2022).
15. Grizzle, R.; Ward, K.; Geselbracht, L.; Birch, A. Distribution and Condition of Intertidal Eastern Oyster (*Crassostrea Virginica*) Reefs in Apalachicola Bay Florida Based on High-Resolution Satellite Imagery. *J. Shellfish Res.* **2018**, *37*, 1027. [CrossRef]
16. Garvis, S.K.; Sacks, P.E.; Walters, L.J. Formation, Movement, and Restoration of Dead Intertidal Oyster Reefs in Canaveral National Seashore and Mosquito Lagoon, Florida. *J. Shellfish Res.* **2015**, *34*, 251–258. [CrossRef]
17. Garvis, S.; Donnelly, M.; Hernandez, E.; Walters, L.; Weishampel, J.; Brockmeyer, R. Remote Sensing of Live and Dead Intertidal Oyster Reefs Using Aerial Photo Interpretation in Northeast Florida. *J. Coast. Conserv.* **2020**, *24*, 1–11. [CrossRef]
18. Windle, A.E.; Poulin, S.K.; Johnston, D.W.; Ridge, J.T. Rapid and Accurate Monitoring of Intertidal Oyster Reef Habitat Using Unoccupied Aircraft Systems and Structure from Motion. *Remote Sens.* **2019**, *11*, 2394. [CrossRef]
19. Collin, A.; Dubois, S.; James, D.; Houet, T. Improving Intertidal Reef Mapping Using UAV Surface, Red Edge, and near-Infrared Data. *Drones* **2019**, *3*, 67. [CrossRef]
20. Espriella, M.C.; Lecours, V.; Frederick, P.C.; Camp, E.V.; Wilkinson, B. Quantifying Intertidal Habitat Relative Coverage in a Florida Estuary Using UAS Imagery and GEOBIA. *Remote Sens.* **2020**, *12*, 677. [CrossRef]
21. Chand, S.; Bollard, B. Low-Cost Remotely Piloted Aircraft System (RPAS) with Multispectral Sensor for Mapping and Classification of Intertidal Biogenic Oyster Reefs. *Aeronaut. Aerosp. Open Access J.* **2020**, *4*, 148–154. [CrossRef]
22. le Bris, A.; Rosa, P.; Lerouxel, A.; Cognie, B.; Gernez, P.; Launeau, P.; Robin, M.; Barillé, L. Hyperspectral Remote Sensing of Wild Oyster Reefs. *Estuar. Coast. Shelf Sci.* **2016**, *172*, 1–12. [CrossRef]
23. Grabowski, J.H.; Powers, S.P. Habitat complexity mitigates trophic transfer on oyster reefs. *Mar. Ecol. Prog. Ser.* **2004**, *277*, 291–295. [CrossRef]
24. Humphries, A.T.; Peyre, M.K.; Decossas, G.A. The Effect of Structural Complexity, Prey Density, and “Predator-Free Space” on Prey Survivorship at Created Oyster Reef Mesocosms. *PLoS ONE* **2011**, *6*, e28339. [CrossRef]
25. Margiotta, A.M.; Shervette, V.R.; Hadley, N.H.; Plante, C.J.; Wilber, D.H. Species-Specific Responses of Resident Crabs to Vertical Habitat Complexity on Intertidal Oyster Reefs. *J. Exp. Mar. Biol. Ecol.* **2016**, *477*, 7–13. [CrossRef]
26. Colden, A.M.; Latour, R.J.; Lipcius, R.N. Reef Height Drives Threshold Dynamics of Restored Oyster Reefs. *Mar. Ecol. Prog. Ser.* **2017**, *582*, 1–13. [CrossRef]
27. Hanke, M.H.; Posey, M.H.; Alphin, T.D. The Influence of Habitat Characteristics on Intertidal Oyster *Crassostrea Virginica* Populations. *Mar. Ecol. Prog. Ser.* **2017**, *571*, 121–138. [CrossRef]
28. Lavan, B. Examining the effect of interstitial space on Eastern oysters (*Crassostrea virginica*): Applications of photogrammetry and Three-Dimensional Modeling. Master’s Thesis, James Madison University, Harrisonburg, VA, USA, 2019. Available online: <https://commons.lib.jmu.edu/master201019/615> (accessed on 16 March 2022).
29. Westoby, M.J.; Brasington, J.; Glasser, N.F.; Hambrey, M.J.; Reynolds, J.M. Structure-from-Motion” Photogrammetry: A Low-Cost, Effective Tool for Geoscience Applications. *Geomorphology* **2012**, *179*, 300–314. [CrossRef]
30. Seymour, A.C.; Ridge, J.T.; Rodriguez, A.B.; Newton, E.; Dale, J.; Johnston, D.W. Deploying Fixed Wing Unoccupied Aerial Systems (UAS) for Coastal Morphology Assessment and Management. *J. Coast. Res.* **2018**, *34*, 704. [CrossRef]
31. Seymour, A.C.; Ridge, J.T.; Newton, E.; Rodriguez, A.B.; Johnston, D.W. Geomorphic Response of Inlet Barrier Islands to Storms. *Geomorphology* **2019**, *339*, 127–140. [CrossRef]
32. Straub, J.A.; Rodriguez, A.B.; Luettich, R.A.; Moore, L.J.; Itzkin, M.; Ridge, J.T.; Seymour, A.C.; Johnston, D.W.; Theuerkauf, E.J. The Role of Beach State and the Timing of Pre-Storm Surveys in Determining the Accuracy of Storm Impact Assessments. *Mar. Geol.* **2020**, *425*, 106201. [CrossRef]

33. DiGiacomo, A.E.; Bird, C.N.; Pan, V.G.; Dobroski, K.; Atkins-Davis, C.; Johnston, D.W.; Ridge, J.T. Modeling Salt Marsh Vegetation Height Using Unoccupied Aircraft Systems and Structure from Motion. *Remote Sens.* **2020**, *12*, 2333. [[CrossRef](#)]
34. Gray, P.C.; Ridge, J.T.; Poulin, S.K.; Seymour, A.C.; Schwantes, A.M.; Swenson, J.J.; Johnston, D.W. Integrating Drone Imagery into High Resolution Satellite Remote Sensing Assessments of Estuarine Environments. *Remote Sens.* **2018**, *10*, 1257. [[CrossRef](#)]
35. Ridge, J.T.; Gray, P.C.; Windle, A.E.; Johnston, D.W. Deep Learning for Coastal Resource Conservation: Automating Detection of Shellfish Reefs. *Remote Sens. Ecol. Conserv.* **2020**, *6*, 431–440. [[CrossRef](#)]
36. Agrafiotis, P.; Skarlatos, D.; Georgopoulos, A.; Karantzalos, K. DepthLearn: Learning to Correct the Refraction on Point Clouds Derived from Aerial Imagery for Accurate Dense Shallow Water Bathymetry Based on SVMs-Fusion with LiDAR Point Clouds. *Remote Sens.* **2019**, *11*, 2225. [[CrossRef](#)]
37. Kim, K.; Lecours, V.; Frederick, C.P. Using 3D micro-geomorphometry to quantify interstitial spaces of an oyster cluster. *PeerJ Prepr.* **2019**, *7*, e27596v1. [[CrossRef](#)]
38. Grabowski, J.H.; Hughes, A.R.; Kimbro, D.L.; Dolan, M.A. How habitat setting influences restored oyster reef communities. *Ecology* **2005**, *86*, 1926–1935. [[CrossRef](#)]
39. Powers, S.P.; Peterson, C.H.; Grabowski, J.H.; Lenihan, H.S. Success of Constructed Oyster Reefs in No-Harvest Sanctuaries: Implications for Restoration. *Mar. Ecol. Prog. Ser.* **2009**, *389*, 159–170. [[CrossRef](#)]
40. Calvert, J.; Strong, J.A.; Service, M.; McGonigle, C.; Quinn, R. An Evaluation of Supervised and Unsupervised Classification Techniques for Marine Benthic Habitat Mapping Using Multibeam Echosounder Data. *ICES J. Mar. Sci.* **2015**, *72*, 1498–1513. [[CrossRef](#)]
41. Hastie, T.; Tibshirani, R. Generalized Additive Models. *Stat. Sci.* **1986**, *1*, 297–318. [[CrossRef](#)]
42. Ridge, J.T.; Rodriguez, A.B.; Joel Fodrie, F.; Lindquist, N.L.; Brodeur, M.C.; Coleman, S.E.; Grabowski, J.H.; Theuerkauf, E.J. Maximizing Oyster-Reef Growth Supports Green Infrastructure with Accelerating Sea-Level Rise. *Sci. Rep.* **2015**, *5*, 14785. [[CrossRef](#)]
43. Nestlerode, J.A.; Luckenbach, M.W.; O’Beirn, F.X. Settlement and survival of the oyster *Crassostrea virginica* on created oyster reef habitats in Chesapeake Bay. *Restor. Ecol.* **2007**, *15*, 273–283. [[CrossRef](#)]
44. Joyce, K.E.; Duce, S.; Leahy, S.M.; Leon, J.; Maier, S.W. Principles and Practice of Acquiring Drone-Based Image Data in Marine Environments. *Mar. Freshw. Res.* **2019**, *70*, 952–963. [[CrossRef](#)]
45. Zarzar, C.M.; Dash, P.; Dyer, J.L.; Moorhead, R.; Hathcock, L. Development of a Simplified Radiometric Calibration Framework for Water-Based and Rapid Deployment Unmanned Aerial System (Uas) Operations. *Drones* **2020**, *4*, 17. [[CrossRef](#)]
46. Lenihan, H.S.; Peterson, C.H. Peterson Conserving Oyster Reef Habitat by Switching from Dredging and Tonging to Diver-Harvesting. *Fish. Bull.* **2004**, *102*, 298–305.
47. Frost, N.J.; Burrows, M.T.; Johnson, M.P.; Hanley, M.E.; Hawkins, S.J. Measuring Surface Complexity in Ecological Studies. *Limnol. Oceanogr. Methods* **2005**, *3*, 203–210. [[CrossRef](#)]
48. Janowski, L.; Wroblewski, R.; Rucinska, M.; Kubowicz-Grajewska, A.; Tysiac, P. Automatic Classification and Mapping of the Seabed Using Airborne LiDAR Bathymetry. *Eng. Geol.* **2022**, *301*, 106615. [[CrossRef](#)]
49. Hogan, S.; Reidenbach, M.A. Quantifying and Mapping Intertidal Oyster Reefs Utilizing LiDAR-Based Remote Sensing. *Mar. Ecol. Prog. Ser.* **2019**, *630*, 83–99. [[CrossRef](#)]
50. Choe, B.H.; Kim, D.J.; Hwang, J.H.; Oh, Y.; Moon, W.M. Detection of Oyster Habitat in Tidal Flats Using Multi-Frequency Polarimetric SAR data. *Estuar. Coast. Shelf Sci.* **2012**, *97*, 28–37. [[CrossRef](#)]